TÜBİTAK

Turkish Journal of Earth Sciences

http://journals.tubitak.gov.tr/earth/

Research Article

Turkish J Earth Sci
(2022) 31: 137-152

doi:10.3906/yer-2112-25

The active fault pattern based on morphotectonic and structural data in the south of Ulubat Lake and the Susurluk valley along the southern branch of North Anatolian Fault Zone: A criticism of the bend model in northwest Anatolia

Gürol SEYİTOĞLU*, Korhan ESAT
Department of Geological Engineering, Tectonics Research Group, Ankara University, Ankara, Turkey

Received: 29.12.2021 • **Accepted/Published Online:** 10.03.2022 • **Final Version:** 29.03.2022

Abstract: Field observations and morphotectonic evaluations on the south of Ulubat Lake and the Susurluk valley show that the dominant active fault pattern consists of northeast-southwest and east northeast-west southwest right-lateral faults and northwest-southeast normal faults developing between these strike-slip faults. We redefined the active faults in the south of Ulubat Lake and discovered that these northeast-southwest right-lateral faults control the route of Susurluk River. Based on these discoveries and evaluations, we can claim that the "bend model" previously proposed for the region is not valid, as seen in the Mustafakemalpaşa Fault and Balıkesir-Kepsut Fault examples. Instead, we suggest that the faults belonging to the southern branch of the North Anatolian Fault Zone extend to Akhisar and İzmir via Bursa, Susurluk, and Balıkesir.

Key words: Neotectonics, North Anatolian Fault Zone, Southern Marmara, active fault

1. Introduction

The North Anatolian Fault Zone (NAFZ) branches off from the west of Bolu and reaches the Aegean Sea via the Sea of Marmara and northwest Anatolia. Although the branches of the NAFZ have been clarified by the seismic reflection studies carried out in the Sea of Marmara (Le Pichon et al., 2001; 2003), there are different opinions in the geological literature about the numbers and locations of the branches in the southern Marmara region (Pavoni, 1961; Şengör et al., 1985; Crampin and Evans, 1986; Barka and Kadınsky-Cade 1988; Barka, 1992; Özalp et al., 2013; Şengör et al., 2014; Seyitoğlu et al., 2016; Emre et al., 2018). Two branches of the NAFZ, one extending from the Sea of Marmara to the Gulf of Saros and the other to the Biga Peninsula via Bursa, are shown in the west of Bolu (Şengör, 1979; Şengör et al., 1985) (Figure 1a). On the other hand, considering the seismic activity in the region, the existence of a third branch extending to İzmir in addition to these two branches is suggested by Crampin and Evans, (1986) (Figure 1b) and also later by Yaltırak et al. (2012) (Figure 1c). This mainly strike-slip fault-related seismic activity is explained with the existence of İzmir – Balıkesir Transfer Zone and no relationship with the NAFZ is described (Ring et al. 1999; Uzel and Sözbilir, 2008; Uzel et al., 2013) (Figure 1d). In fact, the idea of the three-branched NAFZ originates from Pavoni's (1961) tectonic map, where the NAFZ has three branches, and the southern branch is separated from the north of Mudurnu by two parallel faults drawn in the Susurluk valley (Figure 1e). Barka and Kadinsky-Cade (1988) and Barka (1992) also defined the NAFZ by dividing it into three branches (Figure 1f). Based on morphotectonic data, Seyitoğlu et al. (2016) revised this three-branched configuration by stating that the southern branch of the NAFZ splits in Bolu via Mudurnu and Gölpazarı. This branch extends southwest through Bursa, Susurluk, Balıkesir, Akhisar, and Manisa to İzmir and then to the Aegean islands (Seyitoğlu and Esat, 2019; Seyitoğlu et al., 2020a, b, and c).

Unlike the views briefly mentioned above, the tectonic model describing the active faults in northwest Anatolia on the Active Fault Map of Turkey (Emre et al., 2013) suggests that there are five fault bends in northwest Anatolia from north to south (Emre et al., 2018) (Figure 1g). The northernmost two of these, the Central Marmara Bend and the South Marmara Bend form the branches of the NAFZ (Özalp et al., 2013), and the Manyas-Bursa Bend, which is further south of them, includes the Eskişehir Fault Zone by being evaluated outside the NAFZ. Naturally, it is seen that the Balıkesir Bend and the Southern Boundary Bend, which are further south, do not have a structural

* Correspondence: seyitoglu@ankara.edu.tr

relationship with the NAFZ (Emre et al., 2018) (Figure 1g). The bend model (Emre et al., 2018) associates structures such as the Edremit Fault, Yenice-Gönen Fault, and Bursa Fault, which were attributed to the NAFZ in previous studies (Şengör et al., 1985; Barka and Kadinsky-Cade, 1988; Barka,1992; Selim and Tüysüz, 2013; Seyitoğlu et al., 2016), with the relatively secondary structure, the Eskişehir Fault Zone. Evaluation of the fault zones in different regional tectonic models causes differences in the assessment of earthquake hazard analyses of many settlements, such as Bursa, the fourth largest city of Turkey. Therefore, it is important to examine different views about the number of branches and routes of the NAFZ in northwest Anatolia and to evaluate it in the light of new observations.

Using field observations on active faults in the Susurluk valley and south of Lake Ulubat, this article will present the dominant active fault pattern and make a critique of the bend model, showing how the southern branch of the NAFZ extends to the Aegean Sea (Figure 2a).

2. South of Ulubat Lake

2.1 Dorak-Durumtay Fault (DDF)

The Dorak-Durumtay Fault (DDF) is separated from the Ulubat-Doğanköy Fault (UDF) with right stepping in the north of Dorak settlement and extended to the southwest of Durumtay (Seyitoğlu et al., 2021; Figure 2b, c, and d). The eastern part of the DDF was named the Ulubat Fault by Emre et al. (2011a, b) and the western segment of the Ulubat Fault by Karabacak et al. (2021a).

The eastern end of the DDF, which is approximately east-west trending in the south of Ulubat Lake, turns to a northeast-southwest direction in the north of Dorak. Kinematic data from the fault planes in this area display thrust components, as would be expected from a leftward bending of a right-lateral strike-slip fault (Figures 2b and 3a-f). Additional kinematic data were obtained on the DDF around the Ayazköy settlement towards the west (Figures 2b, 2d and 3g-i). To the north of Doğancı settlement (Figure 2d), the DDF creates 2.6 km right-lateral diversion on the Mustafakemalpaşa Çayı (Stream). Further to the west, the DDF reaches the north of Yumurcaklı by passing between the north of Taşkamış Tepe (Hill) and the south of Zambak Tepe and Turna Tepe (Figure 2d). These hills are on a morphologically elongated ridge. The displacement between Taşkamış Tepe and Zambak Tepe is approximately 2.6 km, which is equivalent to a right-lateral offset on the Mustafakemalpaşa Çayı (Figure 2d). The DDF offsets the Susurluk River (Hanife Dere) 4.38 km right lateral to the southwest of the Durumtay settlement, and another short segment offsets the Çiçekli Dere (Creek) 1.15 km right lateral to the south of Beyköy (Figure 2c).

2.2 Mustafakemalpaşa Fault (MPF)

This fault was mapped as the southeast end of the Manyas Fault by Şaroğlu et al. (1992), and then Emre et al. (2011a, b) defined the same fault with a new name which is the northwest-southeast trending right-lateral Mustafakemalpaşa Fault (MPF). According to this definition, the northwest end of the MPF passes through the northeast foothills of the Tokmak Tepe uplift and is located inside the Mustafakemalpaşa settlement, without any displacement on the Mustafakemalpaşa Çayı and continues between the Keltaş and Aralık settlements (Emre et al., 2011a). Further east, the MPF gains an approximately east-west direction between Güller and Kabulbaba (Emre et al., 2011b) and passes into the right-lateral strike-slip Orhaneli Fault with en echelon short segments (Emre et al., 2011c). Contrary to the Emre et al. (2011a), other researchers Selim and Tüysüz (2013) and Selim et al. (2013) draw the MPF to the south of the Tokmak Tepe uplift in the west northwest-east southeast direction, and thus they tried to explain the right-lateral offset along the Mustafakemalpaşa Çayı. The study of Kop et al. (2016) in the east of Mustafakemalpaşa settlement at two different locations, Lalaşahin and Aralık trenches, confirms the northwest-southeast right-lateral strike-slip faults of Emre et al. (2011a).

However, we did not find any kinematic data indicating strike-slip faulting at the northwest end of the MPF. Therefore, there is no kinematic evidence to draw the MPF in the northwest-southeast direction at the northeast slopes of Tokmak Tepe uplift. Instead, we drew the western end of the MPF in an approximately east-west direction using the bends of the streams south of Güllüce (Figure 2b, d). This new position of the fault explains the 830 m right-lateral offset in the Mustafakemalpaşa Çayı (see also the similar interpretation of Selim et al., 2013). Continuation of the MPF to the east passes through the Lalaşahin trench reported by Kop et al. (2016). The fault, following the mountain-piedmont junction south of Üçbeyli, has developed shear zones parallel to the fault here and provides kinematic data for the right-lateral strike-slip faulting in the marble quarry east of Çördük (Figure 4). The en echelon segment of the MPF is morphologically quite prominent in the northeast of Çördük (Figure 2d).

2.3 Keltaş Fault (KTF)

We defined this fault using the fault planes outcropping south and northwest of Keltaş Tepe. The KTF consists of northwest-southeast trending northeast and southwest dipping normal fault segments (Figures 2d and 5).

The northeast dipping normal fault segments are in the northwest of Keltaş Tepe, and the step-like topography here descends from Sakar Tepe to the Quaternary plain where the Aralık settlement is located (Figures 2d and 5a-f). This raises the question of the compressional data attributed to

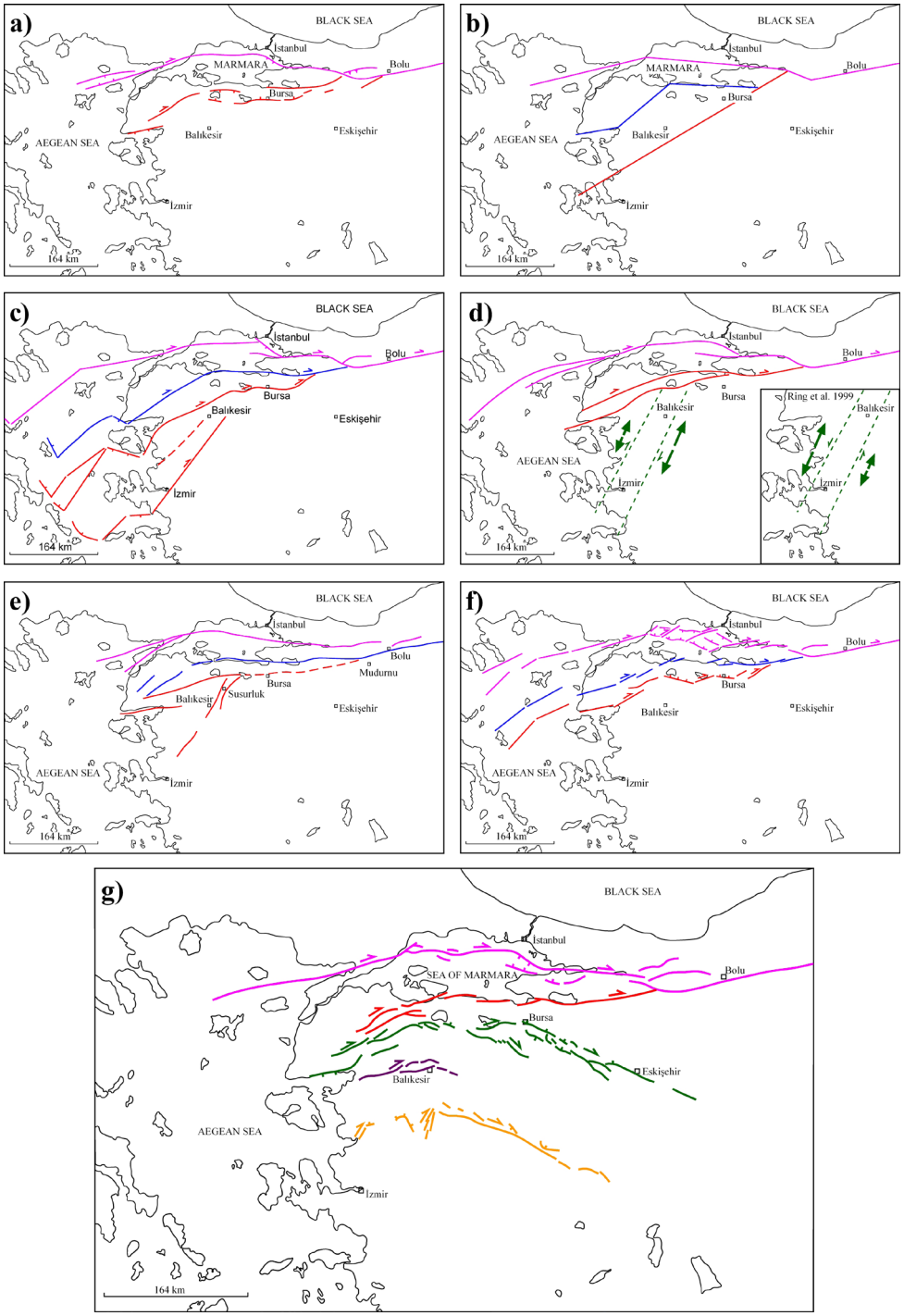

Figure 1. Different views about the locations and numbers of the branches of NAFZ in northwest Anatolia, southern Marmara region. a) Two branched NAFZ from Şengör et al. (1985). b) Three branched NAFZ from Crampin and Evans (1986). c) Three branched NAFZ in western Turkey and Aegean Sea from Yaltırak et al. (2012). d) Right-lateral (Uzel and Sözbilir, 2008; Uzel et al., 2013) or left-lateral (Ring et al., 1999) İzmir-Balıkesir Transfer Zone. e) NAFZ in northwest Anatolia in the tectonic map of Pavoni (1961). Note that the NAFZ has three branches and the faults drawn in the Susurluk valley. f) Three branched NAFZ from Barka and Kadinsky-Cade (1988) and Barka (1992) with segment details. g) The bend model of Emre et al. (2018). Central Marmara Bend/northern branch of the NAFZ: Fuchsia lines; South Marmara Bend/southern branch of the NAFZ: Red lines; Manyas-Bursa Bend: Green lines; Balıkesir Bend: Purple lines; Southern Boundary Bend: Orange lines.

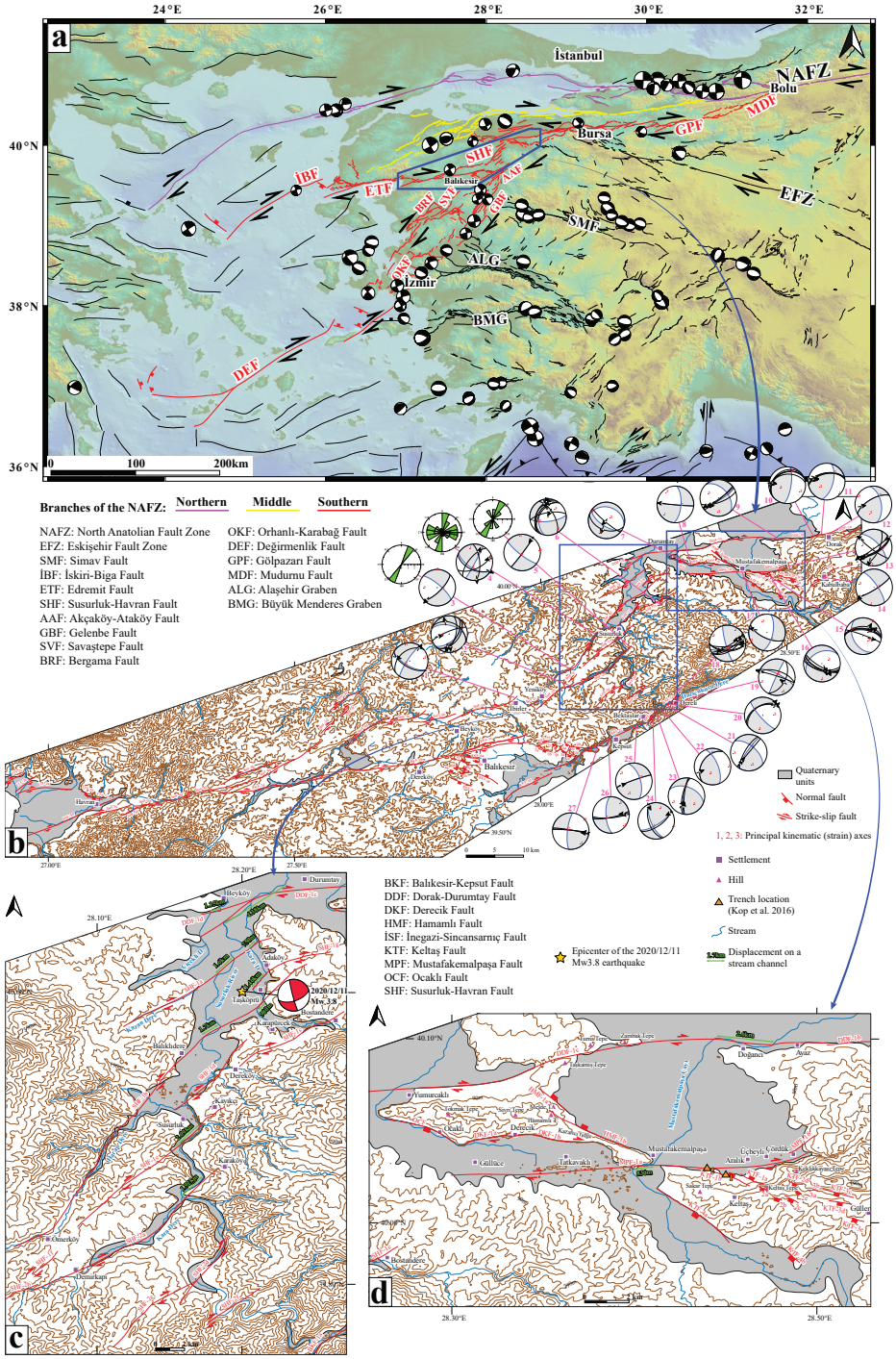

Figure 2. a) The branches of NAFZ in western Turkey and Aegean Sea. After Seyitoğlu et al., (2016); Seyitoğlu and Esat, (2019); Seyitoğlu et al., (2020a). Black fault lines from Barrier et al. (2004); Emre et al. (2013); Caputo and Pavlides (2013); Seyitoğlu et al. (2022). Focal mechanism solutions from Tan et al. (2008), Global CMT Catalogue, Seyitoğlu et al. (2020a, b, c) b) Active faults are from this study and Seyitoğlu et al. (2020a). See Emre et al. (2011a, b, d), Sözbilir et al. (2016), Sümer et al. (2018), and Koçyiğit and Gürboğa (2021) for alternative fault configurations. Contour lines were derived from the 3-arc-second SRTM data. Quaternary units are from Konak (2002) and Türkecan and Yurtsever (2002). The circles represent the equal area lower hemisphere spherical projection of the fault planes and slickenlines. Gray (contractional) and white (extensional) areas and blue circles belong to the fault plane solution obtained by kinematic analysis of the fault data using FaultKin software (Marrett and Allmendinger, 1990; Allmendinger et al., 2012). See Table for numerical data. Rose diagrams show the directions of fractures without striae. c) Fault map of the Susurluk valley. The focal mechanism solution is from Seyitoğlu et al. (2020c). d) Fault map of the Mustafakemalpaşa region.

Table. Fault kinematic data from the field. We used FaultKin software (Marrett and Allmendinger, 1990; Allmendinger et al., 2012) to determine the kinematic axes. N: Normal, T: Thrust. See Figure 2b for graphical representations.

Field data								Kinematic (strain) axes						
			Fault plane		Striae			S1		S2		S3		
#	Latitude (°N)	Longitude (°E)	Strike (°)	Dip (°)	Trend (°)	Plunge (°)	Slip	Trend (°)	Pl. (°)	Trend (°)	Pl. (°)	Trend (°)	Pl. (°)	Photo
1	39.773550	27.947396	120 232	62 42	285 37	26 13	T N	345	8	237	66	79	23	
2	39.797903	28.059862	295 40 15 33 248	37 45 60 55 78	344 189 176 187 258	30 27 30 32 39	N N N N T	166	4	73	34	262	56	Figure 7i-m
3	39.832160	28.059722	45	72	220	14	N	358	3	94	67	267	23	Figure 7a-c
4	39.903786	28.110835	65 355 115 220	60 66 55 66	75 173 118 20	17 5 4 38	T N N N	34	22	202	62	78	17	
5	39.878424	28.180987	37	87	38	11	T	352	10	202	79	83	6	Figure 7g-h
6	39.961797	28.244801	220 210 200 215 330 260	45 35 35 52 62 70	351 0 355 359 344 28	37 19 17 37 24 65	N N N N T T	142	13	244	43	39	44	Figure 7d-f
7	40.049832	28.295333	130 110	82 45	220 200	82 45	N N	207	18	300	7	51	70	Figure 6c-e
8	40.042722	28.304400	95	88	274	25	N	227	16	99	65	322	19	
9	40.095564	28.485817	50 55 70	82 85 70	219 229 239	54 50 28	N N N	181	22	69	44	290	39	
10	40.102501	28.553767	263 230 245 240	40 22 28 31	283 278 277 279	16 17 16 21	T T T T	248	55	17	24	118	24	Figure 3g-i
11	40.106639	28.570298	258 263 258	51 51 55	282 293 280	26 32 28	T T T	232	51	41	39	135	5	Figure 3e-f
12	40.106479	28.586661	240	65	260	36	T	200	45	33	44	297	7	Figure 3a-d
13	40.040374	28.497031	60 58 61 55 25 126	64 69 70 85 65 80	237 227 223 55 194 303	6 26 40 0 22 17	N N N T N N	188	1	96	54	279	36	Figure 4c-e
14	40.019161	28.570927	58	80	235	15	N	191	3	91	72	282	17	

Field data								Kinematic (strain) axes						
			Fault plane		Striae			S1		S2		S3		
#	Latitude (°N)	Longitude (°E)	Strike (°)	Dip (°)	Trend (°)	Plunge (°)	Slip	Trend (°)	Pl. (°)	Trend (°)	Pl. (°)	Trend (°)	Pl. (°)	Photo
15	40.020239	28.466734	275	62	56	50	N	32	8	298	29	137	60	Figure 5b-f
			275	55	61	39	N							
			274	57	63	39	N							
			270	46	31	41	N							
			290	85	104	50	N							
16	40.019771	28.467392	120	75	153	64	N	181	15	279	25	63	60	Figure 5g-i
			115	65	157	55	N							
			115	63	159	54	N							
			100	62	139	50	N							
			107	57	145	43	N							
17	40.031390	28.408854	115	65	282	26	N	243	1	152	52	334	38	
18	39.783699	28.272835	90	60	229	49	N	30	21	185	67	296	9	Figure 8a-c
			56	65	67	23	T							
			56	55	68	16	T							
			85	76	86	6	T							
			90	55	96	8	T							
			60	79	69	38	T							
19	39.763820	28.264086	287	62	290	6	N	160	13	11	75	251	8	
			288	85	289	7	N							
			28	50	126	50	T							
20	39.761464	28.260378	245	46	54	11	N	196	20	307	43	88	40	Figure 8d-e
			235	46	43	12	N							
21	39.759237	28.254664	210	72	218	24	T	168	28	21	57	266	15	Figure 8f-g
			220	90	220	40	T							
22	39.747965	28.248927	215	40	248	24	T	204	57	353	30	91	14	
23	39.742314	28.234715	192	72	209	42	T	141	40	354	46	246	17	Figure 8h-i
			186	80	194	39	T							
24	39.732017	28.227868	160	57	334	9	T	16	29	206	61	109	4	
			55	65	61	14	T							
25	39.719108	28.194855	250	85	253	30	T	202	24	61	60	300	17	
26	39.691323	28.137289	85	77	88	15	T	37	24	236	65	131	7	Figure 8j-k
			78	79	84	29	T							
27	39.681999	28.117698	280	85	98	17	T	143	13	294	75	51	7	Figure 8l-m
			275	86	94	12	T							

the strike-slip faulting in the Aralık trench reported in the Kop et al. (2016) article, suggesting the possibility of soil creep or landslide toe or argilliturbation as demonstrated in a trench on Ulubat Fault (Özaksoy, 2018).

Normal fault planes cropping out just south of Keltaş Tepe are dipping to the southwest (Figures 2d and 5g-i), and they are creating step-like topography between Keltaş Tepe and Koca Dere valley. The normal fault segments around Keltaş Tepe and Güller are evaluated as structures related to the releasing stepover between two right-lateral strike-slip faults called the MPF and the İnegazi-Sincansarnıç Fault (İSF) (Figure 2b).

2.4 Hamamlı (HMF) and Ocaklı (OCF) Faults

In the southwest of Ulubat Lake, the parallelogram-shaped Tokmak Tepe uplift, on which Tokmak Tepe and Sivri Tepe are located, is bounded on the northeast and southwest margins by the Hamamlı and Ocaklı normal faults, and on the north and south by the right-lateral strike-slip DDF and Derecik Fault (DKF), respectively (Figure 2b, 2d). The northwest-southeast trending northeast-dipping fault segments of Hamamlı Fault (HMF) in the northeast of the uplift are drawn using the step-like topography between Hamamlı Tepe and Melde Tepe, and although they do not contain any structural data, the northeast-dipping distinctive fracture surfaces within the agglomerates are attributed to normal faulting (Figure 6a, b).

The prominent topographic difference on the southwest margin of the Tokmak Tepe uplift may correspond to the Ocaklı normal fault (OCF). In the Ocaklı settlement, there are distinct fracture planes within the agglomerates. The position of shear cleavages developed with these surfaces shows that the fracture planes are related to normal faulting (Figure 6c, d, and e).

2.5 Derecik Fault (DKF)

The Derecik Fault (DKF) bounds the Tokmak Tepe uplift from the south and consists of two segments (Figures 2b, 2d, and 6f). This fault, extending semiparallel to the MPF, forms right bends in the stream channels in the west of Derecik, with a displacement of up to 115 m, and with a diversion of up to 335 m in the east of Derecik. The elongated position of the Kazancı ridge in the north of Tatkavaklı settlement is a morphologically important feature indicating strike-slip faulting (Figures 2d and 6f).

3. Susurluk valley

3.1 Susurluk-Havran Fault (SHF)

The SHF-1a segment, which forms the northeast end of the northeast-southwest trending SHF, is evident in the northwest of Adaköy with 1.6 km and 750 m right-lateral displacements on both the Susurluk River and Kara Dere, respectively. The southwest end of the segment is located in the linear Kazan Dere (Figure 2b, 2c). The 29 km long SHF-1b segment, located en echelon to the SHF-1a segment, causes a right-lateral offset of 1.7 km and 980 m, respectively, on both the Susurluk River and Kara Dere in the south and southwest of Taşköprü settlement (Figure 2c). Further southwest in Balıkdere, the segment SHF-1b, which creates a right-lateral offset of 100 m, follows the Harap Dere route and reaches the north of Ömerköy (Figure 2c). The structural data and cataclastic zone are clearly observed on the fault plane west of Ömerköy (Figure 7a-c). It is possible to see shear surfaces and secondary fractures developed parallel to the SHF-1c segment located between Bostandere and Dereköy in the quarry southeast of Karapürçek (Figure 7d-f). The en echelon segment SHF-1d has created a 150 m right-lateral displacement on Acıcasu, which joins the Susurluk River in the southwest of Dereköy (Figure 2c). After segment SHF-1d produces a right-lateral offset of 100 m on the stream joining the Susurluk River further southwest, it creates an abrupt bend in the Susurluk River to the north of the Susurluk settlement, followed by a sudden bend on the Koca Dere (Figure 2c). The SHF-1e, a northeast-southwest trending en echelon segment between Kayıkçı and north of Ömerköy, creates a 2.09 km right-lateral displacement on the Susurluk River (Figure 2c). Similarly, the segments SHF-2a and SHF-2b lying between Karaköy and Yeniköy are characterized both morphologically by creating a 1.92 km dextral offset on the Susurluk River (Figures 2b, 2c and 7g-h) and by following the linear Kara Dere valley further southwest (Figure 2c). Well-developed fault surfaces belonging to the SHF-2a and SHF-2b segments in the quarry at the southwest of Demirkapı present right-lateral strike-slip structural data (Figures 2c and 7i-m). The right stepping of the SHF-2b and SHF-2c segments around İbirler pass to the SHF-3a segment and SHF extends to Havran (Figure 2b). The route of the Susurluk River is controlled by other en echelon segments SHF-2d, SHF-2e, and SHF-2f (Figure 2b, 2c). The greatest right-lateral displacement of the Susurluk River in northwest Anatolia has occurred along with the Balıkesir-Kepsut Fault segments (Figure 2b).

3.2 Balıkesir-Kepsut Fault (BKF)

The distribution of the segments of the BKF shows that the Balıkesir plain should be considered as a pull-apart basin (Seyitoğlu and Esat, 2019). The segments of BKF located in the southwest are connected to the SHF, and the one in the northeast is responsible for the most significant right-lateral offset in the Susurluk River (Figure 2b). In this section, segment distribution and field observations in the northeastern part of the BKF will be given.

The most northeastern end of the BKF is located in the linear valley of Darıçukuru Dere (BKF-1a). Structural data, indicating the right-lateral strike-slip fault, were compiled from five different locations on this segment or on shear zones semiparallel to this segment (Figures 2b and 8a-g). The en echelon segment BKF-1b is also located on a linear valley that hosts the Susurluk River. Its slopes close to the

valley floor provide structural data (Figures 2b and 8h- i). The BKF-1c segment, which can be traced as a single section from Bektaşlar settlement to the Balıkesir Plain, contains structural data indicating the right-lateral strike-slip fault character in the west and northeast of Kepsut (Figures 2b and 8j-m). These field observations and morphotectonic data prove the existence of active northeast-southwest trending faults in the east of Balıkesir that have not been shown in the active fault map of Emre et al. (2011d). The greatest right-lateral displacement of the Susurluk river, 17.32 km, occurred along with these segments, and most likely, the river follows the existing fault line (Figure 2b). Semiparallel to the segments of BKF (BKF-1a, BKF-1b, and BKF-1c), the seismically active (i.e. 2019.12.10 earthquake; ML = 5.0) en echelon Akçaköy-Ataköy Fault (AAF), connects with the right-lateral strike-slip faults located further south, southwest such as Gelenbe Fault (GBF), Savaştepe Fault (SVF), and Bergama Fault (BRF) (Figure 2a) (Seyitoğlu et al. 2020a, b).

4. Discussion

4.1 Age of active faults

A dramatic increase of boron content in the dated core samples from the Ulubat Lake leads the researchers to conclude that the drainage system of the southern Marmara, which eroded the boron deposits, is established not older than 300 ka (Kazancı et al., 2014). When this information and our observation of the fault-controlled course of Susurluk River are taken into account together with the recent U-Th dating from fault-hosted calcite (i.e. 381 ka from Ulubat Fault and 697-156 ka from SHF near Havran) (Karabacak et al. 2021b), it can be concluded that we are dealing with the faults initiated during Middle Pleistocene in the study area.

4.2 South of Ulubat Lake

The south and southeast of Ulubat Lake are morphologically quite distinctive, and it has been shown that the right-lateral strike-slip Ulubat Fault, drawn in an east-west direction in this area, acquires a normal fault character when it turns to the northeast-southwest direction (Emre et al., 2011a, b). This situation is contrary to right-lateral strike-slip kinematics, and our field observations revealed that there is a thrust component on the fault planes in the bend area. This part of the fault section named the western segment of the Ulubat Fault by Karabacak et al. (2021a) is continued further west and redefined as the Dorak-Durumtay Fault (see section 2.1).

The active fault pattern in southern Marmara and northwest Anatolia was determined by Seyitoğlu et al. (2016) with the help of focal mechanism solutions of the earthquakes presented in this article. Accordingly, the northwest-southeast trending faults generally represent normal faulting, while the northeast-southwest and east northeast-west southwest trending ones are in the character of right-lateral strike-slip faults. While the northwest-southeast trending fault in the south of Manyas Lake has been proven to be a normal fault in the trench studies (Kürçer et al., 2017) that is concordant with the regional fault pattern, it has also been confirmed that the northeast-southwest trending faults have right-lateral strike-slip kinematics (Kürçer et al., 2008; 2019).

When viewed at the regional scale, if the normal fault character of the northwest-southeast fault in the south of Manyas Lake is correct, the right-lateral strike-slip character of the MPF with the same trend is kinematically inconsistent. The northwest-southeast trending MPF of Emre et al. (2011a, b), which does not comply with the regional fault pattern, has been tried to be explained with the bend model. The MPF is shown as a northwest-southeast dextral strike-slip fault within the Manyas-Bursa bend (Emre et al., 2018).

When the route of the northwest-southeast trending MPF is examined closely in the maps of Emre et al. (2011a, b), it is seen that it does not cause any offset in the Mustafakemalpaşa Çayı. This situation was also evaluated by Selim et al. (2013), and a new route with an approximately east-west direction was suggested for the MPF. In addition, our field observations provide no structural data indicating strike-slip faulting in the northeast of the Tokmak Tepe uplift which is the so-called northwest-southeast trending route of MPF. Instead, we proposed that the western end of MPF is located on the south of Güllüce with an approximately east-west direction that easily creates distinctive right-lateral shift on the Mustafakemalpaşa Çayı and MPF reaches to the Lalaşahin trench of Kop et al. (2016). Further east, the MPF reaches the south of Çördük settlement by following the mountain-piedmont junction in the north of Keklik Kayası Tepe, in line with the shear zones observed in the quarries south of Üçbeyli village. The quarries to the east of Çördük present structural data in shear zones parallel to the MPF, and the segment of MPF bends in this area and gains a northeast-southwest trend.

Another interesting result of our field observations is to see that the northwest-southeast fault line, passing in Keltaş Tepe and extending to Kabulbaba over Güller, drawn as MPF by the Emre et al. (2011a, b) and confirmed by the Aralık trench of Kop et al. (2016) is not of strike-slip character.

Structural data obtained from the fault surfaces reveal that the structures shown as strike-slip faults in figure 4c of Kop et al. (2016) to the west of Keltaş Tepe are the normal faults dipping northeast, and the faults to the south of Keltaş Tepe are normal faults dipping southwest. For this reason, a new fault named as Keltaş Fault (KTF) has been determined and it is thought that it is developed in the area

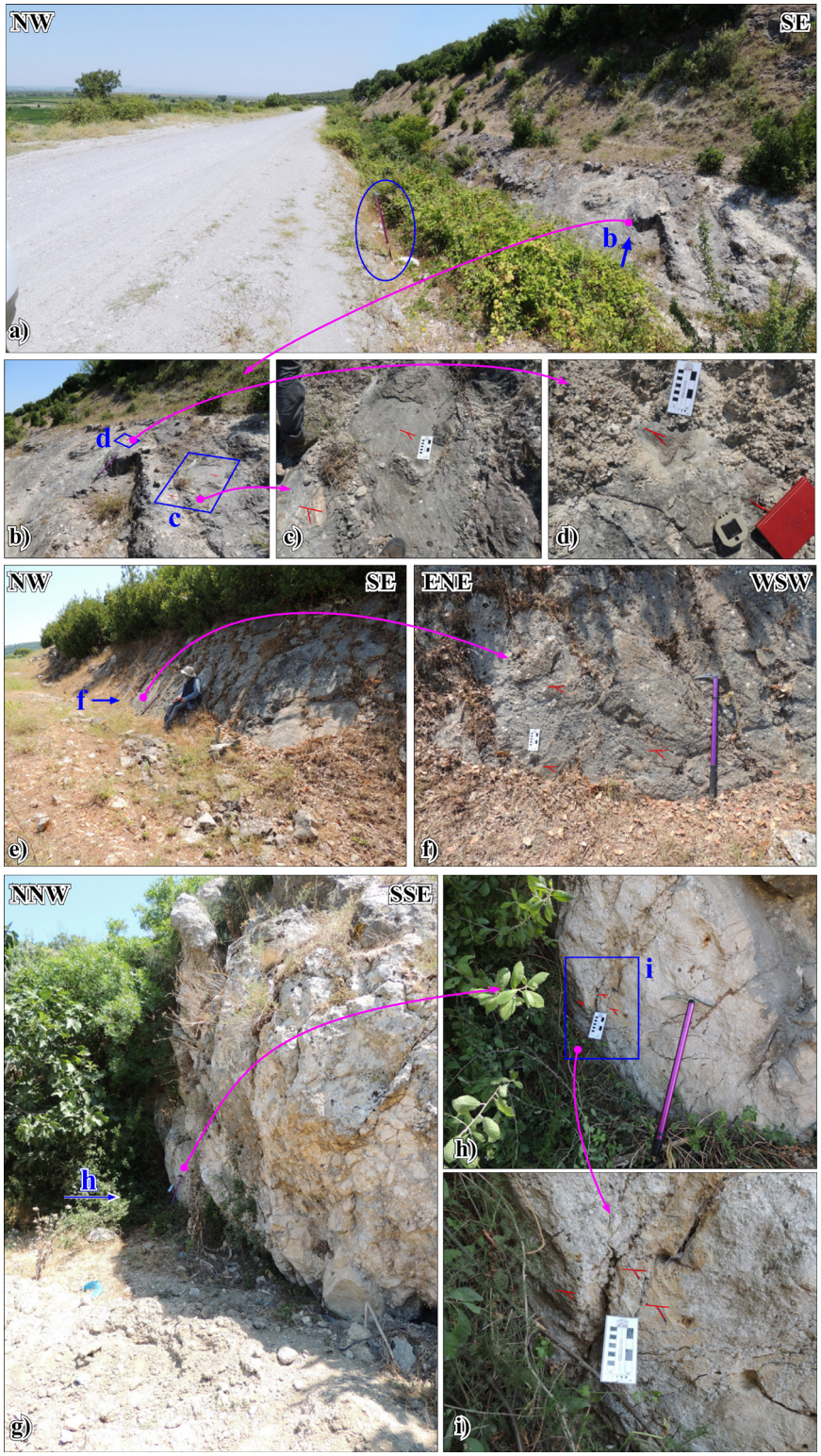

Figure 3. a-f) The right-lateral strike-slip data with thrust component from Dorak-Durumtay Fault (DDF) in the bending location from east-west to northeast-southwest directions. The length of the ice axe is 80 cm. g-i) The right-lateral strike-slip data with reverse component near the slight restraining bend along DDF in the west of Ayaz. See Table and Figure 2b for locations and stereonets.

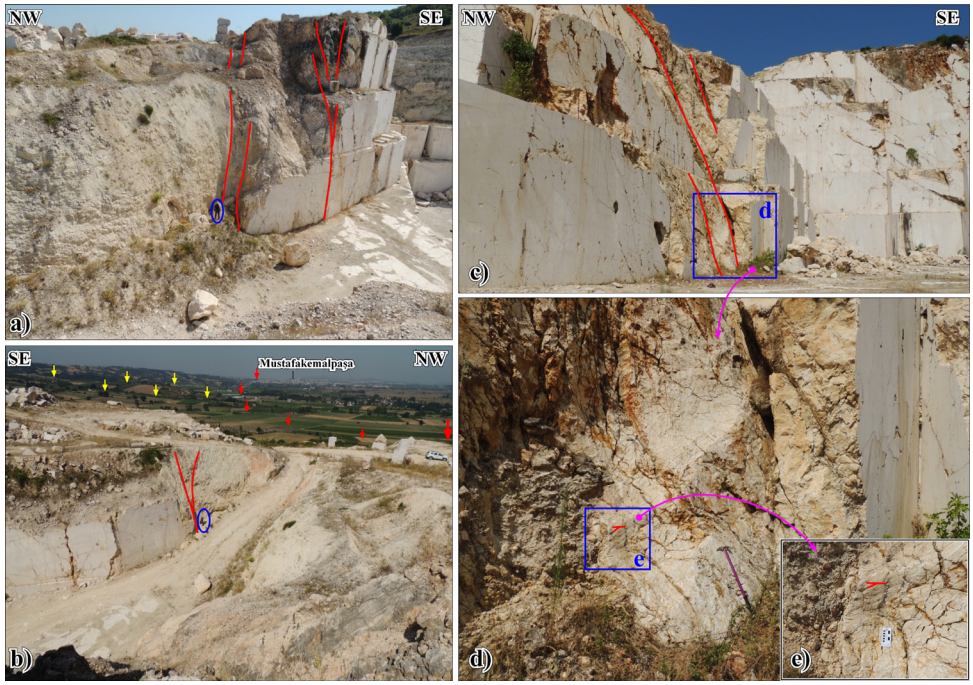

Figure 4. a-b) The east northeast-west southwest shear zone parallel to the MPF (red arrows) in the marble quarry south of Üçbeyli. The height of the geologist in the blue ellipse is 1.72 m. c-e) The right-lateral structural data from the shear zones parallel to the MPF in the marble quarry east of Çördük. See Table and Figure 2b for locations and stereonets.

of releasing stepover between MPF and İnegazi-Sincansarnıç Fault (İSF) (Figure 2b). Our field observations presented and discussed here state that the bend model of Emre et al. (2018) is not valid as seen in the MPF example.

4.3 Susurluk valley

Emre et al. (2011d) described the Susurluk Fault, which is only a north-south trending west- dipping normal fault within the Susurluk valley. The Balıkesir Fault and the Havran-Balya Fault Zone, which are located in the south of Susurluk Fault, make a bend without merging each other and terminate in the south of Kepsut (Emre et al., 2011d). These two faults were defined as the Balıkesir Bend by Emre et al. (2018). On the other hand, our morphotectonic and structural data obtained in the Susurluk valley demonstrate that the route of Susurluk River and its semiparallel streams are completely controlled by the northeast-southwest trending segments of the SHF. In addition, structural data of the northeastern section of the BKF, where the greatest right-lateral displacement of the Susurluk River occurred in northwest Anatolia, are presented, and the existence of the Balıkesir pull-apart basin, not the Balıkesir Bend, was revealed in the region (see section 3.2). The BKF and the en echelon fault segments of the SHF in the Susurluk valley, where seismic activity has been observed recently (Seyitoğlu et al., 2020c), have provided the active fault connection from the south of Ulubat Lake to Balıkesir and from there to the Akhisar Plain and falsify the "bend model" (Emre et al., 2018) in northwest Anatolia. There is also a recent paper providing structural data that the southern branch of NAFZ reaches to Bergama-Aliağa area (Sangu et al., 2020). Moreover, all earthquakes with a magnitude greater than five associated with the Simav Fault, located in the Southern Boundary Bend of Emre et al. (2018), support also our view by providing focal mechanism solutions with pure normal fault kinematics.

5. Conclusions

Our field observations and morphotectonic evaluations in the south of Lake Ulubat and in the Susurluk valley conclude that the dominant active fault pattern in southern Marmara and northwest Anatolia consists of the northeast-southwest and east northeast-west southwest right-lateral strike-slip faults and northwest-southeast trending normal faults developing between these strike-slip faults. As seen in the examples of MPF and BKF described in this paper, the bend model of Emre et al. (2018) is inadequate to explain the pattern of active faulting in northwest Anatolia. In conclusion, the suggestion that the southern branch of NAFZ reaches the Aegean Sea via Bolu, Bursa, Balıkesir, Akhisar, and İzmir appears to be valid (Seyitoğlu et al., 2016; Seyitoğlu and Esat, 2019; Seyitoğlu et al., 2020a, b, c; Sangu et al., 2020).

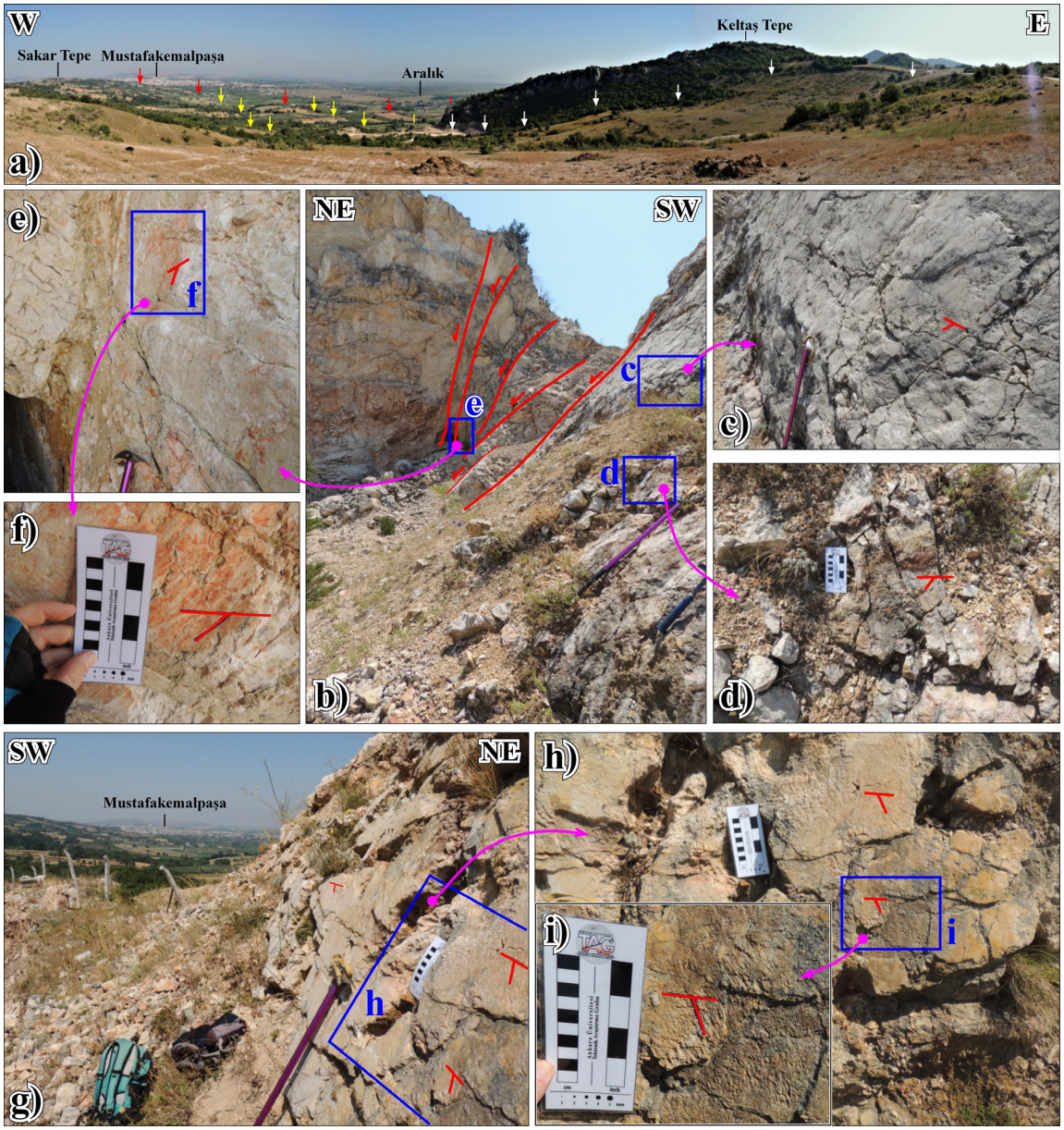

Figure 5. a) The panoramic photo showing the relationship between right-lateral strike-slip MPF (red arrows) and the normal faults of KTF (northeast dipping yellow arrows, southwest dipping white arrows). b-f) The northeast dipping normal fault surfaces of the KTF in the west northwest of Keltaş Tepe. g-i) The southwest dipping normal fault surfaces of the KTF in the south of Keltaş Tepe. See Table and Figure 2b for locations and stereonets.

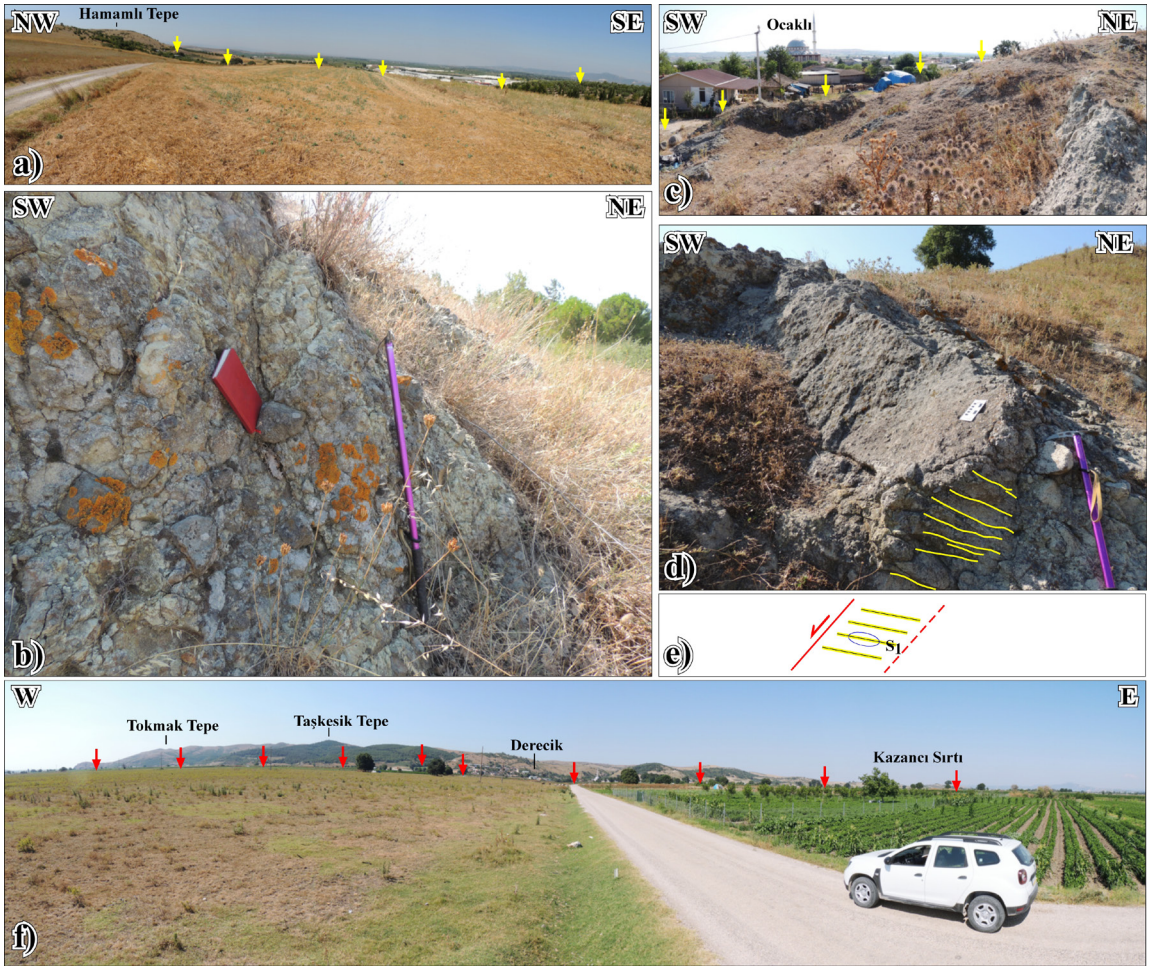

Figure 6. a) The step-like topography in the northeast of Tokmak Tepe uplift. b) The northeast dipping well-developed fracture surfaces. c-e) The southwest dipping fracture surfaces in Ocaklı indicating normal faulting based on shear zone cleavage. See Table and Figure 2b for locations and stereonets. f) A panoramic photo indicating position of the DKF in the south of Tokmak Tepe uplift.

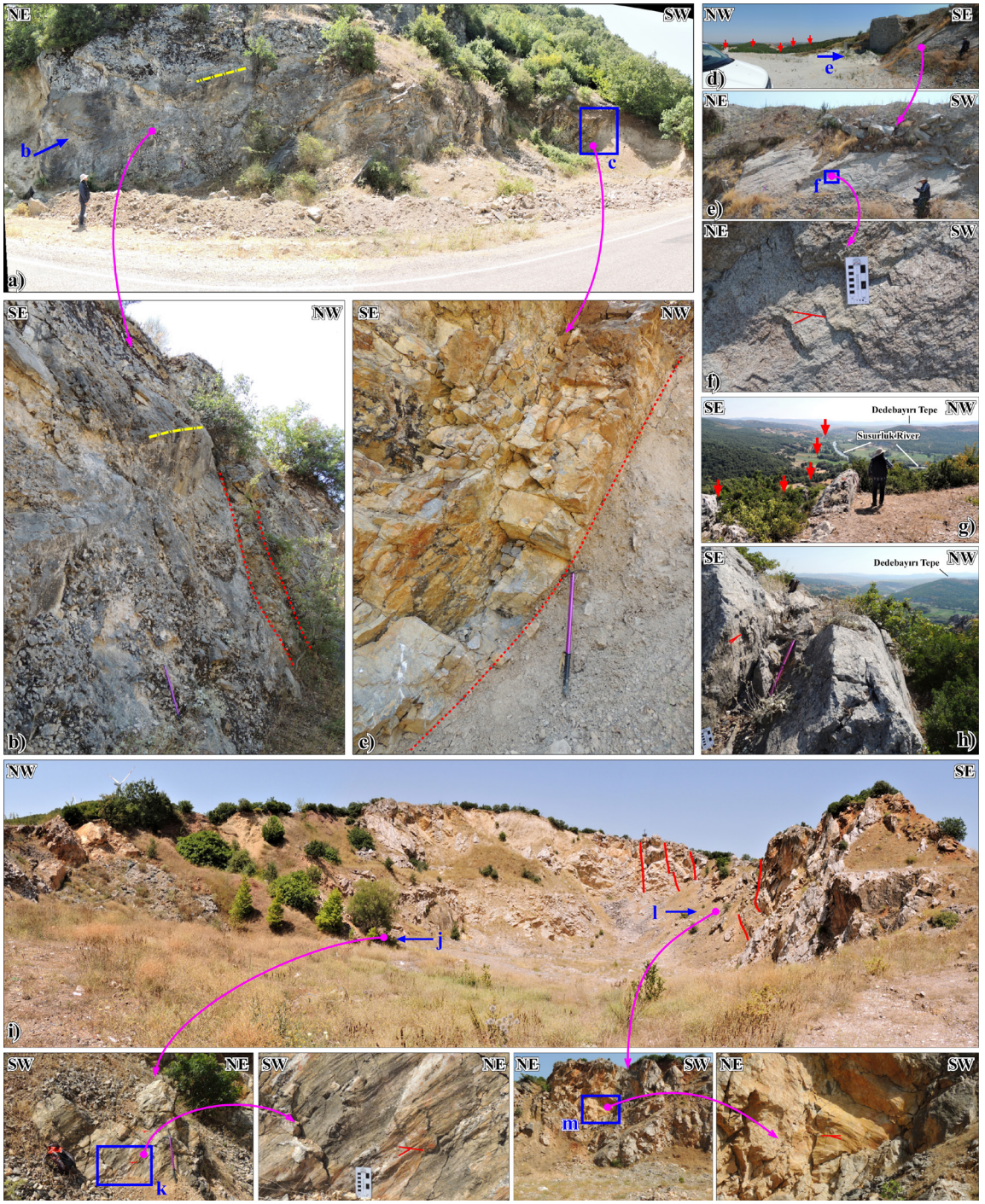

Figure 7. a-c) The northeast-southwest trending right-lateral strike-slip fault surface of the SHF-1b in the west of Ömerköy. d-f) The right-lateral strike-slip data with normal component from a shear zone parallel to the segment SHF-1c southeast Karapürçek. g-h) The right-lateral displacement on the route of Susurluk River along SHF-2a and its parallel shear surfaces at the southwest of Karaköy. i-m) Well-developed fault surfaces with right-lateral strike-slip shear surfaces parallel to the SHF-2a and SHF-2b in the quarry in the west southwest of Demirkapı. See Table and Figure 2b for locations and stereonets.

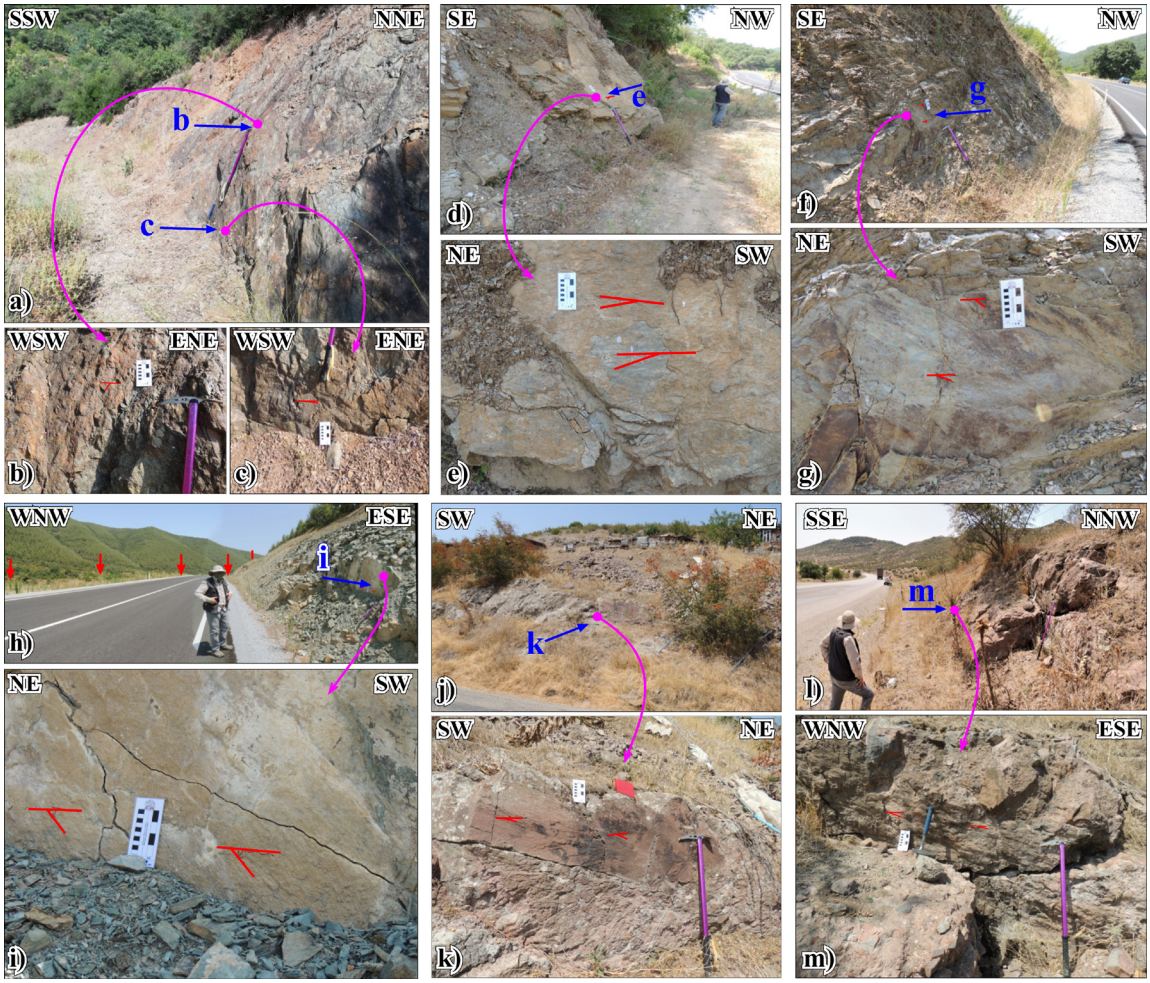

Figure 8. a-c) A shear zone parallel to the BKF-1a in the north of Dereli. d-g) Structural data along the BKF-1a at the southwest of Dereli. h-i) A linear Susurluk Valley and the position of BKF-1b (red arrows) with parallel shear surfaces. j-k) A well-developed shear surface parallel to the BKF-1c in the west of Kepsut. l-m) R-shear of the BKF-1c in the west of Kepsut. See Table and Figure 2b for locations and stereonets.

Acknowledgment
This paper contains partial data from the project report of UDAP-G-18-05 supported by AFAD.

References

Allmendinger RW, Cardozo NC, Fisher D (2012). Structural Geology Algorithms: Vectors and Tensors. Cambridge University Press, 289p.

Barka A (1992). The North Anatolian Fault Zone. Annales Tectonicae 6: 164-195.

Barka A, Kadinsky-Cade K (1988). Strike-slip fault geometry in Turkey and its influence on earthquake activity. Tectonics 7: 663-684.

Barrier E, Chamot-Rooke N, Giordano G (2004). Geodynamic Maps of the Mediterranean-sheet 1: Tectonics and Kinematics. Commission for the Geological map of the World (CGMW) and UNESCO.

Caputo R, Pavlides S (2013). The Greek database of seismogenic sources (GreDaSS), version 2.0.0: A compilation of potential seismogenic sources (Mw>5.5) in the Aegean Region. http://gredass.unife.it/, doi: 10.15160/unife/gredass/0200.

Crampin S, Evans R (1986). Neotectonics of the Marmara Sea region of Turkey. Journal of the Geological Society London 143: 343-348.

Emre Ö, Doğan A, Özalp S, Yıldırım C (2011a). 1:250.000 Scale Active Fault Map Series of Turkey, Bandırma (NK 35-11b) Quadrangle. Serial Number 3, General Directorate of Mineral Research and Exploration, Ankara-Turkey.

Emre Ö, Doğan A, Duman TY, Özalp S (2011b). 1:250,000 Scale Active Fault Map Series of Turkey, Bursa (NK 35-12) Quadrangle. Serial Number 9, General Directorate of Mineral Research and Exploration, Ankara-Turkey.

Emre Ö, Duman TY, Özalp S (2011c). 1:250,000 Scale Active Fault Map Series of Turkey, Kütahya (NJ 35-4) Quadrangle. Serai Number 10, General Directorate of Mineral Research and Exploration, Ankara-Turkey.

Emre Ö, Doğan A, Özalp S (2011d). 1:250.000 Scale Active Fault Map Series of Turkey, Balıkesir (NJ 35-3) Quadrangle. Serial Number 4, General Directorate of Mineral Research and Exploration, Ankara-Turkey.

Emre Ö, Duman TY, Özalp S, Elmacı H, Olgun Ş, Şaroğlu F (2013). Active Fault Map of Turkey with and Explanatory Text 1:1,250,000 scale. General Directorate of Mineral Research and Exploration, Special Publication Series 30.

Emre Ö, Duman TY, Özalp S, Şaroğlu F, Olgun Ş et al. (2018). Active fault database of Turkey. Bulletin of Earthquake Engineering 16: 3229-3275.

Karabacak V, Sancar T, Sağlam Selçuk A, Büyükdeniz Y (2021a). Paleoseismicity of the Ulubat Fault: Inferences on Seismic Behaviour of the Southern Branch of the North Anatolian Fault Zone, South Marmara. Turkish Journal of Earthquake Research 3: 1-19.

Karabacak V, Sançar T, Yıldırım G, Uysal IT (2021b). When did the North Anatolian fault reach southern Marmara, Turkey? Geology: https://doi.org/10.1130/G49726.1.

Kazancı N, Emre Ö, Erturaç K, Leroy SAG, Öncel S et al. (2014). Possible incision time of the large valleys in southern Marmara region, NW Turkey. Bulletin of the Mineral Research and Exploration 148: 1-17.

Koçyiğit A, Gürboğa Ş (2021). Active tectonics of Gülpinar - Tuzla area (Biga peninsula, NW Turkey): the source of 6th February - 24th March 2017 earthquake cluster. Bulletin of the Mineral Research and Exploration 166: 85-112.

Konak N (2002). 1:500.000 scale Geological map of Turkey. İzmir Sheet No:7. General Directorate of Mineral Research and Exploration, Ankara.

Kop A, Özalp S, Elmacı H, Kara M, Duman TY (2016). Active tectonic and palaeseismological features of the western section of Mustafakemalpaşa Fault, Bursa, NW Anatolia. Geodinamica Acta 28: 363-378

Kürçer A, Chatzipetros A, Tutkun SZ, Pavlides S, Ateş Ö et al. (2008). The Yenice-Gönen active fault (NW Turkey): Active tectonics and palaeoseismology. Tectonophysics 453: 263-275

Kürçer A, Özaksoy V, Özalp S, Güldoğan ÇU, Özdemir E et al. (2017). The Manyas fault zone (southern Marmara region, NW Turkey): active tectonics and paleoseismology. Geodinamica Acta 29: 42-61

Kürçer A, Özalp S, Özdemir E, Uygun Güldoğan Ç, Duman TY (2019). Active tectonic and paleoseismologic characteristics of the Yenice-Gönen fault, NW Turkey, in the light of the 18 March 1953 Yenice-Gönen Earthquake (Ms=7.2). Bulletin of the Mineral Research and Exploration 159: 29-63

Le Pichon X, Chamot-Rooke N, Rangin C (2003). The North Anatolian fault in the Sea of Marmara. Journal of Geophysical Research 108: doi 10.1029/2002JB001862.

Le Pichon X, Şengör AMC, Demirbağ E, Rangin C, İmren C et al. (2001). The active Main Marmara Fault. Earth and Planetary Science Letters 192: 595-616.

Marrett R, Allmendinger RW (1990). Kinematic analysis of fault-slip data. Journal of Structural Geology 12: 973-986.

Özaksoy V (2018). On the distinction of tectonic and nontectonic faulting in palaeoseismological research: a case study from the southern Marmara region of Turkey. International Journal of Earth Sciences 107: 1777-1788.

Özalp S, Emre Ö, Doğan A (2013). The segment structure of southern branch of the North Anatolian Fault and paleoseismological behaviour of the Gemlik Fault, NW Anatolia. Bulletin of the Mineral Research and Exploration 147: 1-17.

Pavoni N (1961). Die Nordanatolische Horizontalverschiebung. Geologische Rundschau 51: 122-139.

Ring U, Laws S, Bernet M (1999). Structural analysis of a complex nappe sequence and late-orogenic basins from the Aegean Island of Samos, Greece. Journal of Structural Geology 21: 1575-1601.

Sangu E, Gürer ÖF, Gürer A (2020). Fault kinematic and Plio-Quaternary paleostress evolution of the Bakırçay Basin, Western Turkey. International Geology Review 62: 1245-1261.

Selim HH, Tüysüz O, Karakaş A, Taş KÖ (2013). Morphotectonic evidence from the southern branch of the North Anatolian Fault (NAF) and basins of the south Marmara sub-region, NW Turkey. Quaternary International 292: 176-192.

Selim HH, Tüysüz O (2013). The Bursa-Gönen Depression, NW Turkey: a complex basin developed on the North Anatolian Fault. Geological Magazine 150: 801-821.

Seyitoğlu G, Kaypak B, Aktuğ B, Gürbüz E, Esat K et al. (2016). A hypothesis for the alternative southern branch of the North Anatolian Fault Zone, Northwest Turkey. Geological Bulletin of Turkey 59: 115-130.

Seyitoğlu G, Esat K (2019). The possible segmentation of the southern branch of the North Anatolian Fault Zone between Bolu and İzmir: A discussion on the suitability of İzmir-Balıkesir Transfer Zone interpretation. 72nd Geological Congress of Turkey, The Proceedings and Abstracts Book, 475-477. ISBN 978-60501-1261-0.

Seyitoğlu G, Kaypak B, Esat K, Çıvgın B (2020a). Seismotectonic evaluation of the 2020.01.22 (Mw=5.5) Musalar-Akhisar earthquake. Technical Report DOI: 10.13140/ RG.2.2. 30307. 50729.

Seyitoğlu G, Kaypak B, Esat K, Koca B (2020b). Contributions of the 2020.10.30 (Mww=7.0) Samos Earthquake and its aftershocks to the understanding of Aegean neotectonic framework. Technical Report DOI: 10.13140/RG.2.2.22233.34403/1.

Seyitoğlu G, Kaypak B, Esat K, Koca B (2020c). Seismic activity in Susurluk Valley: the tectonic meaning of 2020.12.11 (Mw=3.8) Taşköprü earthquake. Technical Report DOI: 10.13140/RG.2.2.31117.97764.

Seyitoğlu G, Esat K, Kaypak B, Çıvgın B, Oruç B et al. (2021). Determination of active faults that are possible earthquake sources around Bursa by geological and geophysical methods. Final report, AFAD Project no UDAP-G-18-05 (in Turkish).

Seyitoğlu G, Tunçel E, Kaypak B, Esat K, Gökkaya E (2022). The Anatolian Diagonal: a broad left-lateral shear zone between the North Anatolian Fault Zone and the Aegean / Cyprus arcs. Geological Bulletin of Turkey 65: https://doi.org/10.25288/tjb.1015537.

Sözbilir H, Özkaymak Ç, Uzel B, Sümer Ö, Eski S, Tepe Ç (2016). Palaeoseismology of the Havran-Balıkesir Fault Zone: evidence for past earthquakes in the strike-slip dominated contractional deformation along the southern branches of the North Anatolian fault in northwest Turkey. Geodinamica Acta 28: 254-272.

Sümer Ö, Uzel B, Özkaymak Ç, Sözbilir H (2018). Kinematics of the Havran-Balıkesir Fault Zone and its implication on geodynamic evolution of the southern Marmara region, NW Anatolia. Geodinamica Acta 30: 306-323.

Şaroğlu F, Emre Ö, Kuşçu İ (1992). Active Fault Map of Turkey. Ankara, Turkey: General Directorate of Mineral Research and Exploration.

Şengör AMC (1979). The North Anatolian transform fault: its age, offset and tectonic significance. Journal of the Geological Society London 136: 269-282.

Şengör AMC, Görür N, Şaroğlu F (1985). Strike-slip deformation basin formation and sedimentation: Strike-slip faulting and related basin formation in zones of tectonic escape: Turkey as a case study. In: Biddle KT, Christie-Blick N (eds) Strike-slip faulting and basin formation. The Society of Economic Paleontologists and Mineralogists Special Publications 37, pp 227-264.

Şengör AMC, Grall C, İmren C, Le Pichon X, Görür N et al. (2014). The geometry of the North Anatolian transform fault in the sea of Marmara and its temporal evolution: implications for the development of intracontinental transform faults. Canadian Journal of Earth Sciences 51: 222-242.

Tan O, Tapırdamaz MC, Yörük A (2008). The Earthquake Catalogues for Turkey. Turkish Journal of Earth Sciences 17: 405-418.

Türkecan A, Yurtsever A (2002). 1:500.000 scale Geological map of Turkey. İstanbul Sheet No:1. General Directorate of Mineral Research and Exploration, Ankara.

Uzel B, Sözbilir H (2008). A first record of a strike-slip basin in western Anatolia and its tectonic implication: The Cumaovası basin. Turkish Journal of Earth Sciences 17: 559-591.

Uzel B, Sözbilir H, Özkaymak Ç, Kaymakçı N, Langereis CG (2013). Structural evidence for strike-slip deformation in the İzmir-Balıkesir transfer zone and consequences for late Cenozoic evolution of western Anatolia (Turkey). Journal of Geodynamics 65: 94-116.

Yaltırak C, İşler EB, Aksu AE, Hiscott RN (2012). Evolution of the Bababurnu Basin and shelf of the Biga Peninsula: Western extension of the middle strand of the North Anatolian Fault Zone, Northeast Aegean Sea, Turkey. Journal of Asian Earth Sciences 57: 103-119.